PAPER

Check for updates

An innovative Ag/Cu-doped polypyrrole hybrid nanocomposite gas sensor for superior ammonia detection at room temperature

Arunima Verma,[a] Tanuj Kumar ●*[a] and Rahul Singhal[b]

Hybrid nanocomposites combining organic and inorganic materials offer enhanced responses to reducing and oxidizing gases. This study presents a novel polypyrrole (PPy)-based hybrid nanocomposite synthesized with varying concentrations of silver (Ag) and copper (Cu) nanoparticles for efficient ammonia sensing at room temperature. The uniform dispersion of Ag/Cu nanoparticles within the PPy matrix enables a dense, smooth surface that enhances electron transport and boosts conductivity, compatibility, and catalytic activity. Structural and surface analyses using XRD, FESEM, UV-vis, EDS, TGA, and FTIR revealed that the PPy@Ag/Cu hybrid nanocomposite sensor achieved an 86% response to 300 ppm ammonia. Selectivity was confirmed against gases like carbon dioxide, carbon monoxide, ethanol, and hydrogen sulphide. The protonation and deprotonation in the PPy@Ag/Cu heterojunction contribute to the ammonia sensing mechanism, making this nanocomposite a promising material for environmental monitoring applications.

1. Introduction

Nanosensors are characterized by remarkable physical properties owing to the significantly high surface area to volume ratio that is unique to nanoscale materials. They provide advantageous performance advantages, such as sensitivity that is orders of magnitude higher than that of conventional sensors, and fast response and response times. Nanosensors can perform as autonomous systems or can be built into integrated systems or networks. Moreover, the extremely small size of the sensing element allows for the building of portable devices. The detection of chemical and biological species is central to many areas of environment health, healthcare, and occupational safety. Many materials have been used as nanosensors for a variety of applications.[1] Among these materials, intrinsically conducting polymers (ICP) have demonstrated immense potential in the field of sensors, energy storage and nanoelectronics, owing to their attractive mechanical, electrical, physical, and structural properties. The advantage of ICPs, as nanosensors, lies in their usability in ambient conditions and room temperature. Further inclusion of a secondary component such as nanoparticles (NPs) in the ICP matrix is another factor that influences the electrical properties of ICPs. This has

led to a surge in research concerning the development of polymer nanocomposites (PNCs) for nanosensor applications. Metals and metallic compounds offer a synergistic effect when combined with ICPs. Metal oxides and metal sulphides have been widely used for the detection of various analytes. Roy *et al.*[2,3] have synthesized a range of polyaniline (PANI) composites with metal oxide and calcium titanate, which exhibit remarkable electronic and electrical properties. Parveen *et al.*[4] have reported a significant response of 90% towards liquefied petroleum gas (LPG) using PANI/TiO_2 nanocomposites. In another study, they reported a highly sensitive PANI/$CaTiO_3$ nanocomposite-based humidity sensor operating in the temperature range of 40–200 °C.[5] However, operations at high temperatures affect the structure and performance of the sensor. Hence, sensors based on ICPs, that are operable at room temperature, can overcome this issue. When combined with NPs, the ICP based sensors show an enhancement in sensitivity and selectivity. The most relevant feature, amongst the properties of ICP that are affected by analyte adsorption, is the electrical property. The parameters that influence the sensor performance are polymerization method, type of oxidants, type of dopants and level of doping, and reaction temperature.[6]

The development of gas sensors with enhanced sensitivity and selectivity at room temperature is critical for applications in environmental monitoring, industrial safety, and healthcare. Ammonia (NH_3), a colourless gas with a pungent odor, is widely used in industrial processes, but it is hazardous at high

[a] *Department of Physics and Astronomical Sciences, Central University of Jammu, 181143, India. E-mail: tanuj.nsm@cujammu.ac.in*

[b] *Department of Physics, Malaviya National Institute of Technology Jaipur, Rajasthan - 302017, India*

concentrations and requires precise monitoring to prevent health risks. Conducting polymers, especially polypyrrole (PPy), have garnered interest in gas sensing applications due to their tunable conductivity, chemical stability, and high response to various gases at room temperature. However, PPy alone may suffer from limitations in sensitivity, stability, and selectivity. To address these issues, doping with metal nanoparticles, such as silver (Ag) and copper (Cu), has emerged as a promising approach to enhance the gas-sensing performance of PPy. Ag/Cu hybrid nanocomposites are recognized for their unique catalytic and electronic properties, which can significantly improve the sensor's response to ammonia gas.[7] Silver possesses high electrical conductivity and catalytic activity, while copper can enhance charge transfer processes and improve adsorption sites for NH_3 molecules. The combination of these two metals within a PPy matrix creates a synergistic effect that improves electron transfer and increases the effective surface area for gas adsorption. This synergy facilitates a faster and more sensitive response to ammonia gas molecules at ambient conditions, making Ag/Cu-doped PPy nanocomposites highly suitable for room-temperature sensing applications.[8] The Ag/Cu-doped PPy nanocomposite-based gas sensors are fabricated through chemical oxidative polymerization, followed by deposition on silicon substrates. These sensors demonstrate excellent ammonia-sensing performance, attributed to the uniform distribution of Ag and Cu nanoparticles within the PPy matrix, which enables effective interaction between NH_3 molecules and the nanocomposite surface. Furthermore, the Ag/Cu-doped PPy sensors show remarkable stability, rapid response and recovery times, and resistance to interference from humidity variations, enhancing their practical applicability in real-world scenarios.

The selection of materials for ammonia sensing in this study is grounded in a comprehensive set of criteria designed to ensure both high performance and practical applicability. Key among these criteria is the high sensitivity of the materials, particularly PPy and PPy@Ag/Cu hybrid nanocomposites, to ammonia gas. This sensitivity enables the detection of ammonia even at trace concentrations, making the materials suitable for applications where precise monitoring is crucial. Another critical factor is the ability of these materials to function effectively at room temperature, eliminating the need for external heating and reducing energy consumption, which is vital for portable and cost-effective sensor systems. Rapid response and recovery times are equally important, as they enable real-time monitoring and quick detection of changes in ammonia concentration. The selected materials also exhibit excellent selectivity for ammonia, ensuring minimal interference from other gases such as ethanol, carbon monoxide, or hydrogen sulfide. This characteristic is crucial in mixed-gas environments, where cross-sensitivity could lead to inaccurate readings. Additionally, the materials demonstrate robust chemical stability, maintaining their performance even under challenging conditions, such as varying humidity levels and extended periods of operation. The structural and morphological properties of the materials were also critical considerations.

The hybrid nanocomposites feature high porosity and a significant active surface area, facilitating effective gas adsorption and interaction. The incorporation of Ag and Cu nanoparticles further enhances these properties by improving electrical conductivity, creating more active sites, and introducing synergistic effects that amplify the sensing response. The ability to tune the properties of the nanocomposites through controlled doping of Ag and Cu adds another layer of flexibility, allowing for optimization based on specific application needs. Practical factors, such as ease of synthesis, scalability, and cost-effectiveness, were also prioritized to ensure that the materials could be readily produced and deployed on a large scale. Additionally, environmental considerations were taken into account, with efforts made to select materials that are non-toxic and sustainable. To the best of my knowledge, no research has been carried out thus far on the topic of gas sensors based on PPy@Ag/Cu hybrid nanocomposite films, which could improve the room temperature detection performance of ammonia gas.

2. Experimental procedure

2.1 Materials and reagents

The list of chemicals used during the research work is listed in Table 1. No additional purification was performed on the other reagents prior to use. All of the solutions used in the experiment were prepared using double distilled water.

2.2 Synthesis of polypyrrole (PPy)

Polypyrrole (PPy) was synthesized using a method involving the mixing of solutions. Fig. 1 shows the use of ammonium persulfate as an oxidant/initiator in conjunction with pyrrole polymerization in concentrated hydrochloric acid to produce an acidic medium. Pyrrole (1 M) was dissolved in 0.15 M HCl to form pyrrole hydrochloride solution. To this reaction mixture, a solution of ammonium persulfate (0.08 M) that acts as an oxidant was added slowly with continuous stirring at 0–5 °C and the final volume of the solution is 10 mL. After complete addition of the oxidizing agent, the reaction mixture was allowed to stand for 24 h without stirring.[9] The black precipitate of the polypyrrole was recovered by vacuum filtration and washed with acetone and HCl to remove the oligomers and chlorine ions, respectively. The precipitate was dried in an oven for 24 h at 50 °C to achieve constant weight.

Table 1 List of chemicals used during the synthesis process

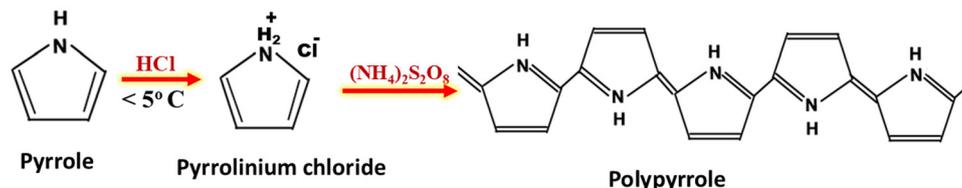| S. no.	Chemical	Formula	Molecular weight (g mol^{-1})
1.	Pyrrole	C_4H_5N	67.091
2.	Hydrochloric acid	HCl	36.46
3.	Ammonium persulfate (APS)	$(NH_4)_2S_2O_8$	228.20
4.	Silver nitrate	$AgNO_3$	169.87
5.	Copper acetate	$Cu(CH_3COO)_2$	181.63

Fig. 1 Synthesis of polypyrrole in acidic medium.

2.3 Synthesis of the PPy@Ag/Cu hybrid nanocomposite

Fig. 2 shows the oxidative polymerization procedure used for preparing the hybrid nanocomposite of polypyrrole (PPy) and metal. Prepare a solution containing 1 M pyrrole monomer dissolved in 0.15 mL of hydrochloric acid. To produce metal salt solutions, dissolve 0.1 g silver nitrate ($AgNO_3$) and copper acetate $Cu(CH_3COO)_2$ separately in 5 mL of distilled water. To produce the desired composition, combine the pyrrole solution with the various metal salt solutions in the appropriate quantities. Stir the mixture thoroughly to ensure it is homogeneous. Add 0.1 g of an oxidizing agent, such as ammonium persulfate (APS), to the mixture of pyrrole and metal salt solutions. The oxidation process proceeds with the polymerization of pyrrole into PPy while also reducing metal ions, resulting in the formation of Ag and Cu nanoparticles inside the matrix. The mixture was stirred until it turned greenish dark brown, suggesting that it had formed a PPy@Ag/Cu hybrid nanocomposite. Filtration apparatus should be used to collect the solid material from the nanocomposite solution. Wash the collected composite thoroughly with distilled water and ethanol to eliminate any unwanted compounds. To eliminate any residual solvent, dry the PPy@Ag/Cu nanocomposite in an oven set to a regulated temperature.[10,11]

PPy@Ag/Cu hybrid nanocomposites were made using varying concentrations of silver nitrate (0.12 M, 0.3 M, 0.59 M, 0.89 M, and 1.19 M) and copper acetate (0.12 M, 0.29 M, 0.56 M, 0.83 M, and 1.11 M), henceforth referred to as PPy@Ag/Cu1, PPy@Ag/Cu2, PPy@Ag/Cu3, PPy@Ag/Cu4, and PPy@Ag/Cu5, respectively as shown in Table 2.

Table 2 PPy with various concentrations of silver nitrate and copper acetate

Sample	PPy (g)	Silver nitrate (g)	Copper acetate
PPy	0.6	0	0
PPy@Ag/Cu1	0.6	0.1	0.1
PPy@Ag/Cu2	0.6	0.25	0.25
PPy@Ag/Cu3	0.6	0.5	0.5
PPy@Ag/Cu4	0.6	0.75	0.75
PPy@Ag/Cu5	0.6	1	1

2.4 Stabilization mechanism of the PPy@Ag/Cu hybrid nanocomposite

When combined with metal ions, the nitrogen atoms in PPy amine and imine groups form a strong bond. By forming a coordination bond with silver or copper, these nitrogen atoms assist in stabilizing the metal nanoparticles within the PPy matrix. A redox reaction involving PPy reducing Ag^+ and Cu^{2+} ions to Cu^0 and Ag^0, respectively, can be used in the synthesis of the hybrid nanocomposite. This process generates metal nanoparticles within the PPy matrix without the need for any external sources.[12] Because of the high electrical conductivity of Ag and Cu, their nanoparticle incorporation into the PPy matrix can enhance its capabilities in this area. This synergistic effect improves the performance of nanocomposite materials in gas sensing and related applications. Fig. 3 shows that the PPy-containing amine groups prevent Ag/Cu nanoparticles from adhering together. The overall reaction can be summarized as follows:
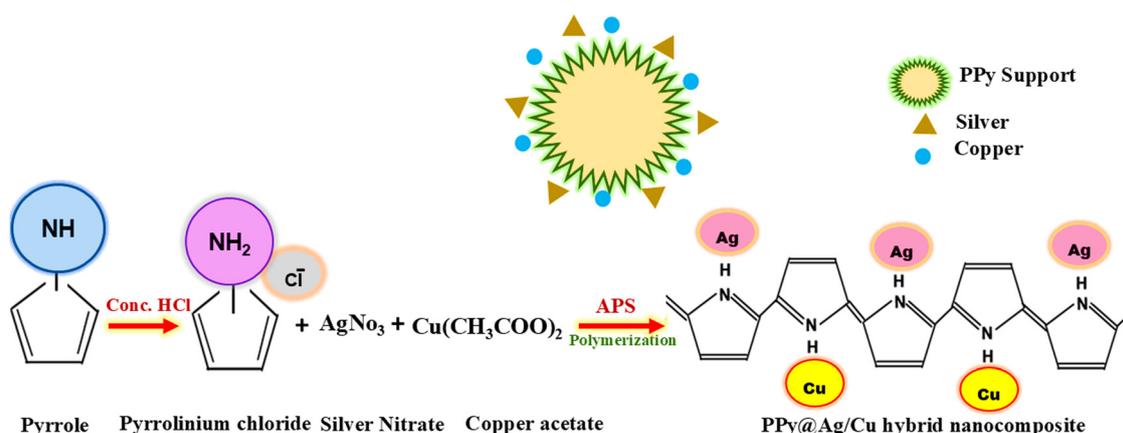

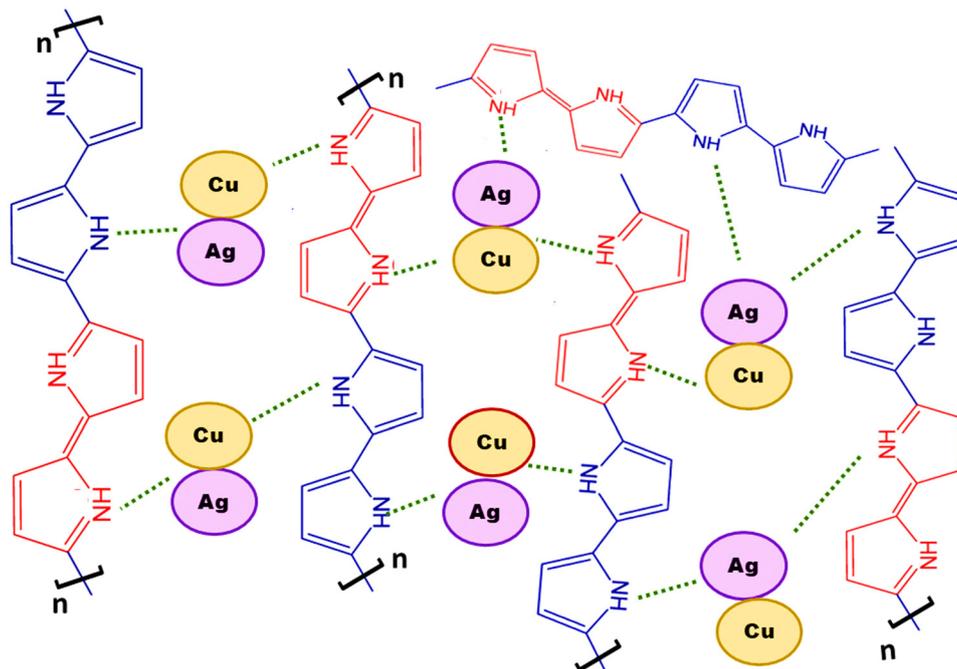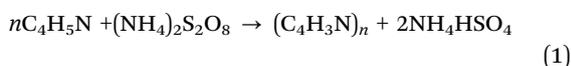**Fig. 2** Synthesis of the PPy@Ag/Cu hybrid nanocomposite.

Fig. 3 Stabilization mechanism of the PPy@Ag/Cu hybrid nanocomposite.

- Oxidative polymerization of pyrrole:

$$nC_4H_5N + (NH_4)_2S_2O_8 \rightarrow (C_4H_3N)_n + 2NH_4HSO_4$$
(1)

- Reduction of Ag and Cu ions:

$$Ag^+ + e^- \rightarrow Ag^0$$
$$Cu^{2+} + 2e^- \rightarrow Cu^0$$
(2)
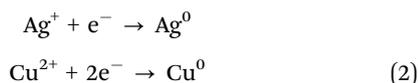
The Ag^+ and Cu^{2+} ions are reduced to their respective metallic states (Ag^0 and Cu^0), forming nanoparticles within the PPy matrix.

Formation of hybrid nanocomposite:

$$(C_4H_3N)_n + Ag^0 + Cu^0 \rightarrow PPy@Ag/Cu \text{ hybrid nanocomposite}$$
(3)

The Ag and Cu nanoparticles provide additional stability through metal–polymer interactions, which help to prevent the degradation of the polymer chains and maintain the structural integrity of the composite. The hybrid structure also enhances the electron transport pathways due to the conductive nature of both PPy and the metal nanoparticles, resulting in improved performance in gas sensors.[13] This stabilization mechanism is crucial for maintaining the nanocomposite functionality over time, especially when exposed to environmental conditions.

2.5 The preparation of the PPy film

When pure polypyrrole is dissolved in *N*-methyl pyrrolidone (NMP), a viscous solution is formed due to the high molecular weight and strong intermolecular interactions of polypyrrole. NMP is a polar aprotic solvent known for its excellent ability to dissolve polymers, particularly those with strong π-conjugated backbones like polypyrrole. The viscosity of the solution is a result of the polymer chains being solvated and extended within the solvent, leading to increased resistance to flow. This viscous nature is crucial for processes such as film coating, where a uniform layer of the polymer is desired. The use of NMP ensures that the polypyrrole is fully dissolved, maintaining the integrity of its molecular structure, which is essential for its application in gas sensors.[1] This solution was used to deposit the PPy layer on a silicon substrate using the spin coating method. The process was carried out at 1500 rpm for 20 seconds. Additionally, silver paste was used to create electrical connections on the PPy film. The width of the track and the gaps between two successive tracks were 1 mm each.

2.6 The preparation of the PPy@Ag/Cu nanocomposite film

In order to create a solution, the prepared sample of PPy@Ag/Cu hybrid nanocomposite, which weighed 2 mg, was dissolved in polyvinyl pyrrolidone at a concentration of 0.1 M. The spin coating method was implemented in order to deposit a layer of PPy@Ag/Cu hybrid nanocomposite onto a silicon substrate. The procedure was carried out at a speed of 1500 rpm for a duration of ten seconds. Additionally, silver paste was used to create an electrical connection between the electrically created film, as shown in Fig. 4.
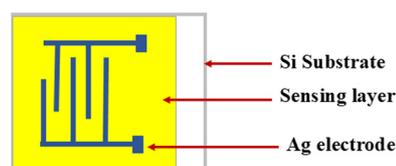

Fig. 4 Schematic diagram of a fabricated PANI@Ag nanocomposite film.

3. Results and discussion

3.1 X-ray diffraction (XRD) studies

Fig. 5 presents the XRD spectra of PPy and PPy@Ag/Cu hybrid nanocomposites with varying Ag/Cu concentrations. The broad peak observed at 25.3° in Fig. 5a is attributed to the amorphous nature of PPy. In addition to this broad peak, the XRD patterns of the PPy@Ag/Cu hybrid nanocomposites display narrow peaks, reflecting the high crystallinity of Ag and Cu nanoparticles. The distinct peaks at 38.15°, 44.01°, 64.11°, and 77.23° correspond to the (111), (200), (220), and (311) lattice planes of the FCC structure of silver. Similarly, the FCC structure of copper is evidenced by sharp diffraction peaks at 43.91°, 50.37°, and 74.49°, representing the (200) and (220) lattice planes. The crystallite size variation with increasing Ag/Cu concentration in the nanocomposite, summarized in Table 3, highlights the influence on crystal growth and nucleation processes. Initially, as the Ag/Cu concentration increases, the crystallite size decreases, likely due to the nanoparticles acting as nucleation sites, which inhibit crystal growth by promoting the formation of smaller crystallites. However, at higher Ag concentrations, the crystallite size increases as the aggregation of Ag nanoparticles facilitates larger crystal growth. This nonlinear trend in crystallite size is a complex interplay of nucleation, aggregation, and growth dynamics. The average crystallite sizes were calculated using Scherrer's equation (eqn (4)):

$$D = \frac{k\lambda}{\beta \mathrm{Cos}\theta} \qquad (4)$$

where λ = 0.154 nm is the wavelength of X-rays for Cu Kα, β is FWHM (full width at half maximum intensity of the peak), θ is the diffraction angle, and D is the crystallite size. Table 3 presents the crystallite size values. Notably, the larger atomic radius of silver compared to copper influences the crystallite size in the hybrid nanocomposite. As shown in Fig. 5b, the XRD peaks shift to the right with increasing Ag/Cu doping in the PPy matrix, indicating changes in lattice parameters.[14] This peak shift is typically associated with lattice contraction, arising from the strain induced by the incorporation of Ag and Cu atoms, which alters the lattice spacing. The strain, Y-axis intercept, and slope were analysed using the Williamson–Hall plot, depicted in Fig. 5(c–f). This method decouples strain and crystallite size contributions to peak broadening, providing insights into the material's microstructure. However, it assumes uniform crystalline deformation, which simplifies the analysis by neglecting spatial strain variations. In reality, silver-copper nanocomposites may exhibit non-uniform strain due to lattice defects and nanoparticle interactions, leading to localized stress and strain variations.

3.2 FT-IR Study

The FTIR data serves as a vital tool for confirming the successful incorporation of Ag and Cu into the PPy matrix and for understanding the resultant changes in the functional properties of the nanocomposite, which are crucial for applications such as gas sensing, where these interactions can significantly affect performance. Fig. 6 shows the prepared nanocomposite FT-IR spectra, and the peaks around 1556 cm^{-1} correspond to C=C stretching vibrations, indicating the conjugated structure of PPy. Additionally, N–H bending vibrations may be observed around 1301 cm^{-1}, confirming the presence of nitrogen in the polymer backbone. The absorption peaks at 868 cm^{-1} and
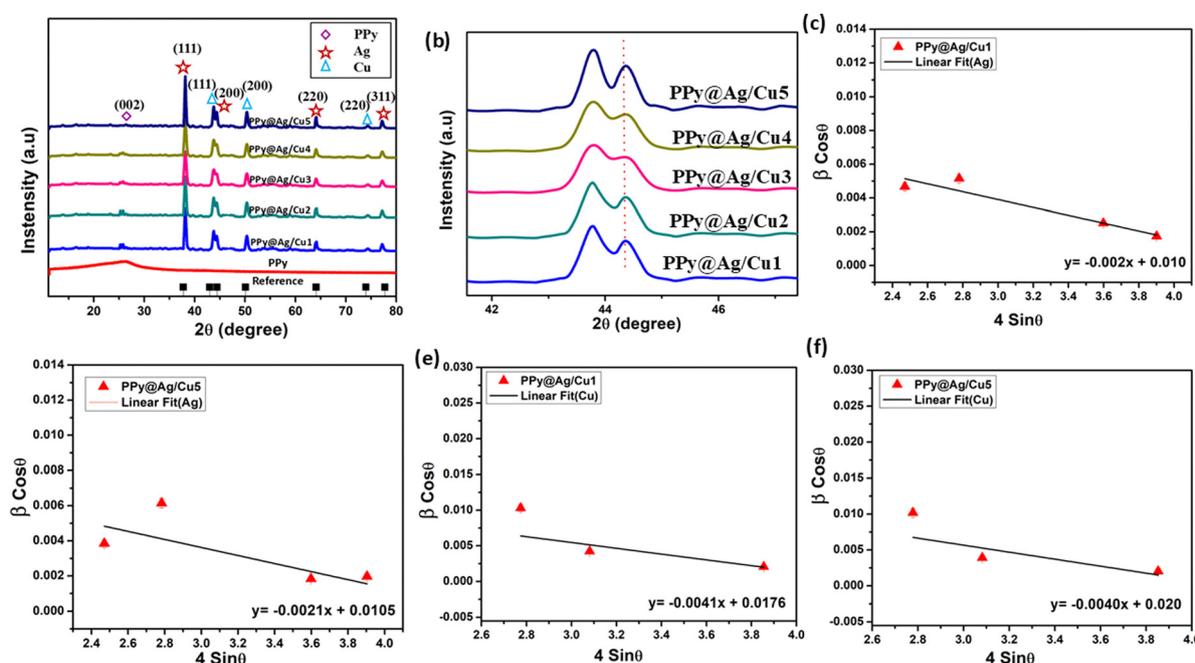

Fig. 5 (a) The XRD spectra of the PPy and PPy@Ag/Cu1–5 hybrid nanocomposite; (b) magnified view of the XRD pattern for the Ag peak shift on the (200) plane of the PPy@Ag/Cu hybrid nanocomposite; (c–f) Williamson–Hall plot of the nano-crystalline silver and copper sample.

Table 3 The calculated crystallite size of the PPy@Ag/Cu hybrid nanocomposite

| Conc. (g)	2θ of the intense peak (degrees)		FWHM of intense peak (β, radians)		Crystallite size (nm)		d-spacing nm		Lattice parameter (a, Å)		Macrostrain ($\varepsilon \times 10^{-3}$)		Dislocation density ($\delta \times 10^{-3}$ nm^{-2})	
	Ag	Cu	Ag	Cu	Ag	Cu	Ag	Cu	Ag	Cu	Ag	Cu	Ag	Cu
0.2	38.15	43.91	0.0051	0.014	24.7	10.4	2.36	2.06	4.08	3.56	4.29	8.87	1.63	9.16
0.5	38.16	43.89	0.0064	0.017	23.3	8.65	2.35	2.06	4.07	3.56	4.54	10.7	1.83	13.3
1	38.17	43.01	0.0071	0.014	20.5	10.1	2.34	2.11	4.08	3.63	5.17	9.30	2.37	9.67
1.5	38.15	43.03	0.0062	0.0016	21.5	10.5	2.34	2.11	4.07	3.63	4.12	8.96	2.15	8.99
2	38.16	43.99	0.0041	0.0015	28.2	10.6	2.35	2.07	4.08	3.56	3.53	8.85	1.10	9.15
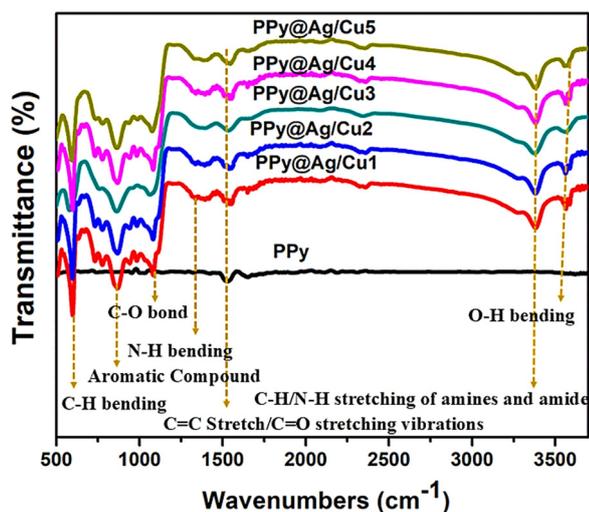
Fig. 6 The FTIR spectra of PPy and the PPy@Ag/Cu hybrid nanocomposite with the concentration ratios of Ag/Cu.

1073 cm^{-1} are due to the aromatic compound and C–O bond. The peak of the C–H/N–H stretching of amines and amide was relocated from 3385 cm^{-1} to 3388 cm^{-1} due to the overlap between the two spectra. The broad feature in the region of 1400–1600 cm^{-1} could indicate surface plasmon resonance associated with the metallic nanoparticles, contributing to enhanced optical properties. We observed slight shifts in the characteristic PPy peaks because to the incorporation of Ag/Cu can reveal changes in the bonding environments. A shift to higher wavenumbers implies a blue shift indicating stronger bonding or interactions with the metals.

3.3 Optical analysis and band gap values

Fig. 7a displays the UV-vis spectra of PPy, revealing a prominent absorption peak at 257 nm. This peak corresponds to the polaron absorption characteristic of conducting PPy.[15] The presence of silver and copper nanoparticles was assessed in the PPy@Ag/Cu hybrid nanocomposite samples by UV-vis absorption, as shown in Fig. 7b. The spectra confirming the presence of the nanoparticles have the highest absorption bands at 206 nm, 207 nm, 208 nm, 209 nm, and 210 nm, respectively, of the silver and copper samples. In terms of absorption intensity, the PPy@Ag/Cu hybrid nanocomposite shows outstanding results. We noticed that at higher

wavelengths, absorption peaks (red shifts) imply material particle size or shape changes. The increased doping concentration of Ag/Cu nanoparticles can lead to stronger interactions between the metal nanoparticles and the matrix. These interactions can alter the electronic environment of the nanoparticles, leading to a reduction in the energy required for electronic transitions.[16] This red shift can also be caused by increased surface plasmon resonance effects, where the collective oscillation of electrons in the metal nanoparticles changes due to altered dielectric properties or inter–particle interactions.

As per Tauc's equation the direct allowed transition type can be used to approximatively determine the optical band gap of powder samples.[17] In order to estimate the band gap, the straight line was extrapolated to the point where $(\alpha h\nu)^2 = 0$. As shown in Fig. 7(c and d), the spectra analysis produced transition bandgaps (E_g) of around 3.2 eV for pure PPy, 3.1 eV for PPy@Ag/Cu1, 2.9 eV for PPy@Ag/Cu2, 2.5 eV for PPy@Ag/Cu3, 2.7 eV for PPy@Ag/Cu4, and 2.8 eV for PPy@Ag/Cu5 hybrid nanocomposites. At low concentrations of doped Ag/Cu in PPy, the band gap typically decreases initially due to enhanced charge carrier mobility and increased interaction between the metal nanoparticles and the polymer matrix. This reduction in the band gap occurs as metal nanoparticles introduce new electronic states near the conduction and valence bands, allowing for easier electron transitions and thus reducing the energy required for these transitions as discussed above. However, as the metal concentration continues to increase, the band gap eventually begins to increase again. This reversal is often attributed to the aggregation or clustering of metal nanoparticles at higher concentrations, which can reduce the effective interaction between the metal and the polymer matrix. Excessive doping can lead to a reduction in free charge carriers and hinder electron transport due to increased scattering and localized defects. Additionally, the higher Ag/Cu content may distort the PPy structural integrity, leading to changes in the electronic environment that ultimately widen the band gap.

3.4 Morphological analysis

Fig. 8 shows the results of a FESEM analysis of PPy and the PPy@Ag/Cu hybrid nanocomposites with varying concentrations of silver and copper doped into the PPy matrix, which allowed us to determine their morphology. Fig. 8(a and d) illustrates that PPy exhibits a spheroidal morphology. The silver and copper particles, created by reducing metal ions in
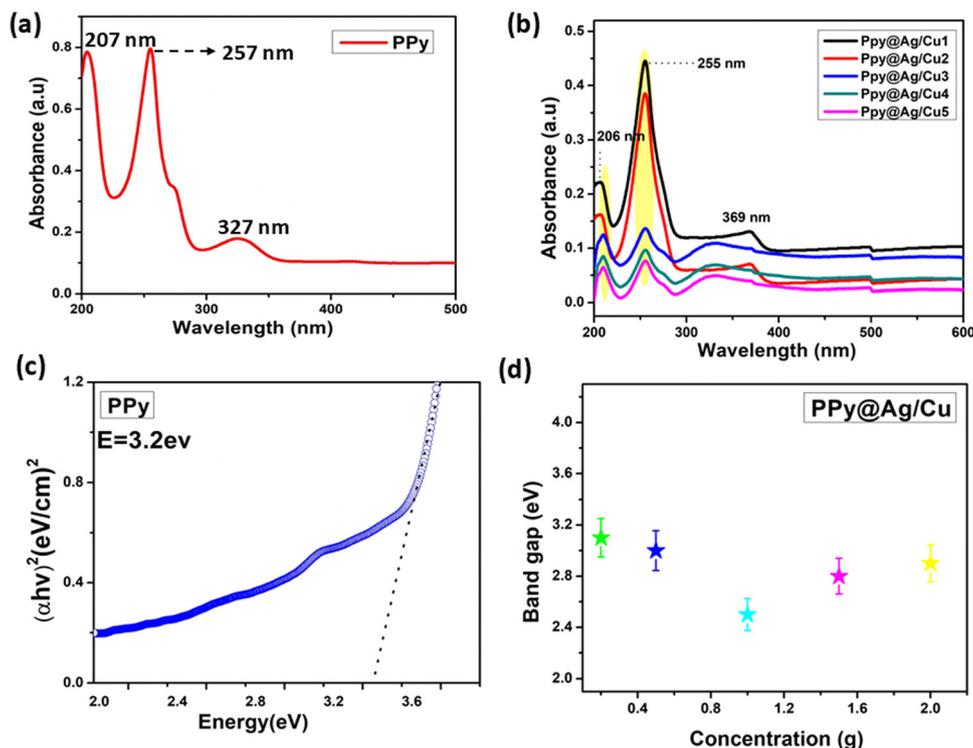
Fig. 7 (a) UV spectrum of (a) PPy and (b) the PPy@Ag/Cu1–5 hybrid nanocomposite; (c) and (d) band gap of PPy and its hybrid nanocomposite with various concentrations of doped metal.
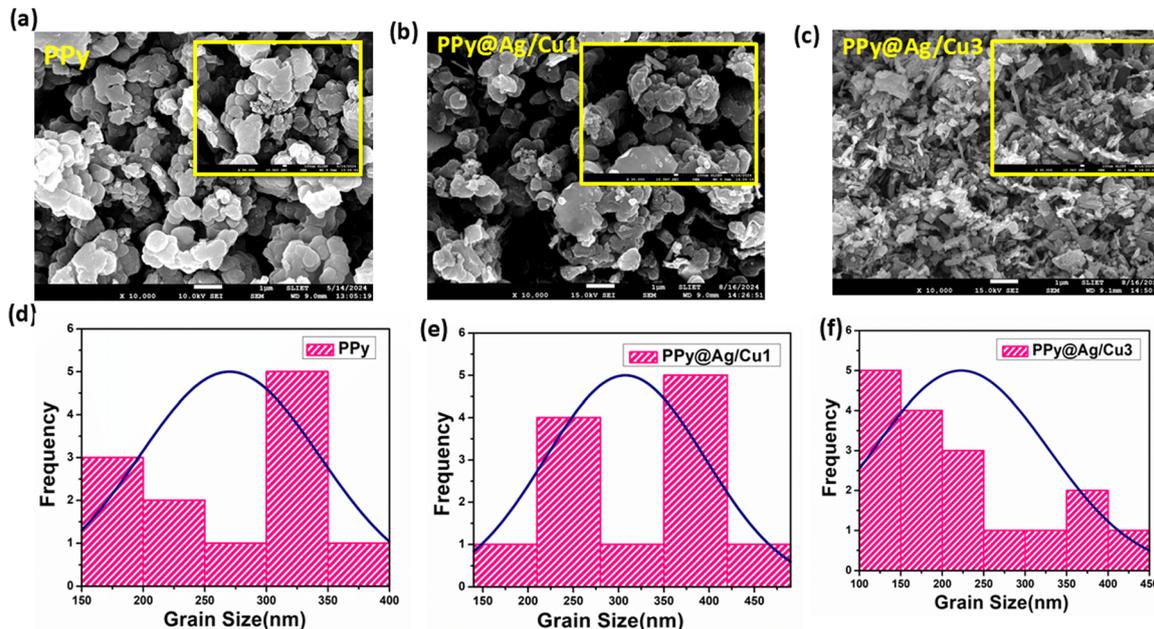

Fig. 8 FE-SEM of (a) PPy; (b–c) PPy@Ag/Cu hybrid nanocomposite with low and high concentration and (d–f) grain size of PPy and its nanocomposites.

hydrochloric acid, seem like an agglomeration of nano spheroids with an average diameter of around 306 nm, as shown in Fig. 8b. Illustrations of PPy@Ag/Cu1 in Fig. 8(b and c) reveal silver and copper nanoparticles that are equally dispersed and

aggregate. The PPy@Ag/Cu5 hybrid nanocomposite, on the other hand, demonstrates how the structural alterations observed in the host metal due to doping might influence the flake particle interactions (Fig. 8c). At higher concentrations of

PPy@Ag/Cu5 hybrid nanocomposite, changes in the crystal structure could occur, impacting the agglomeration propensity. As the concentration of Ag/Cu increases in the PPy matrix, the particle size decreases, as observed in Fig. 8(e and f). This reduction in particle size can be attributed to the presence of Ag and Cu nanoparticles, which act as nucleation sites and inhibit the growth of larger particles. With higher concentrations of Ag/Cu, more nucleation centres are available, leading to the formation of smaller, well-dispersed particles. Additionally, metal nanoparticles like Ag and Cu can induce lattice strain and restrict the coalescence of polymer particles, further contributing to the reduction in particle size. This behaviour is a common feature in nanocomposites, where the introduction of metallic dopants influences the growth dynamics, resulting in finer particles with increased surface area.

The decrease in particle size with increasing Ag/Cu concentration in the PPy matrix significantly enhances the gas sensing performance. Smaller particle size leads to a larger surface area-to-volume ratio, providing more active sites for gas adsorption. This increased surface area allows for a greater interaction between the gas molecules (such as ammonia) and the sensing material, improving the sensitivity of the sensor. Moreover, the presence of Ag and Cu nanoparticles in the matrix promotes better electron transfer and enhances the catalytic activity of the material. These metal nanoparticles can facilitate charge transfer processes between the gas molecules and the PPy matrix, leading to a more pronounced change in the electrical conductivity upon gas exposure. This improved interaction boosts the overall response and detection capability of the gas sensor.

3.5 Dispersive X-ray spectroscopy (EDX)

Fig. 9 presents the EDS analysis of PPy and the PPy@Ag/Cu hybrid nanocomposites with varying Ag/Cu concentrations. In the EDS spectrum of pure polypyrrole (Fig. 9a), carbon (C) and nitrogen (N), which form the backbone of the polymer, are prominently detected. Fig. 9(b and c) clearly shows that silver (Ag) and copper (Cu) nanoparticles are successfully incorporated into the PPy matrix. Visual inspection further confirms the presence of Ag, Cu, N, and C in the PPy@Ag/Cu hybrid nanocomposites at both low and high concentrations of doped nanoparticles. As expected, the hydrogen (H) signal is not observed due to its low-energy nature. Additionally, the

presence of chlorine (Cl) and oxygen (O) is attributed to the use of HCl and ammonium persulfate during the synthesis process.

3.6 Thermogravimetric (TG) and differential thermal analysis (DTA)

In order to comprehend further how ammonia adsorbs and desorbs from the sensor material, TG examines the weight fluctuations. A rise in mass following heating may suggest ammonia desorption, whereas a rise in mass upon cooling may indicate the opposite. Using a dynamic nitrogen flow and a heating rate of 100 °C min^{-1}, along with TGA and DTA experiments, the thermal stability of the synthesized PPy and its hybrid nanocomposites was examined Fig. 10. The TGA curve of PPy (Fig. 10a) exhibits three major weight loss steps. The initial weight loss around 29–94 °C corresponds to the loss of adsorbed moisture and volatile impurities. The second weight loss, occurring between 94–216 °C, is attributed to the decomposition of the polymer backbone and the release of dopant ions. A significant weight loss in this range indicates the degradation of the polymer chains. The third stage, above 330 °C, involves the complete decomposition of the carbonaceous residue, resulting in a stable weight plateau at higher temperatures. The DTA curve of PPy reveals an exothermic peak at around 110 °C, corresponding to the evaporation of adsorbed water (Fig. 10b). A prominent endothermic peak at 310 °C indicates the degradation of the polypyrrole chains. The broad nature of this peak suggests a gradual decomposition process.

The initial weight loss at temperatures below 100 °C is typically attributed to the evaporation of absorbed water or moisture from the PPy@Ag/Cu hybrid nanocomposite (Fig. 10c). This step indicates the hygroscopic nature of the material. A small percentage of weight loss (∼1%) is observed in this region. The first major decomposition stage corresponds to the degradation of the PPy backbone. PPy undergoes thermal decomposition in this temperature range, breaking down into smaller molecules such as volatile byproducts. A significant weight loss around 11% occurs, indicating the decomposition of the polymer matrix. The second major weight loss is due to the further breakdown of the polymer and possible combustion of any residual organic material. At this stage, the material may also start decomposing the PPy, Ag and Cu interactions. Another significant weight reduction of ∼9% occur,
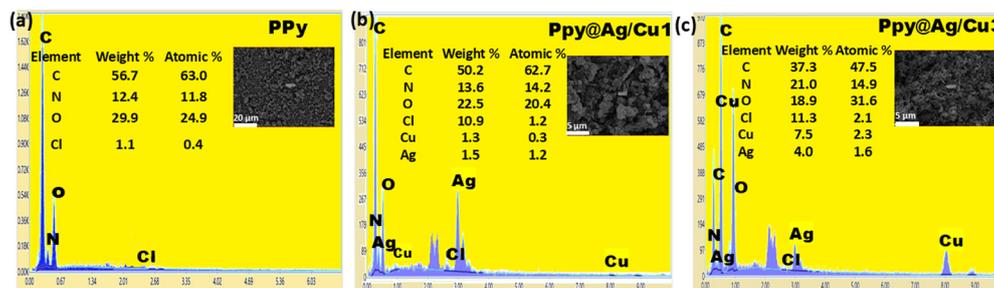

Fig. 9 EDS spectra of (a) PPy and (b) PPy@Ag/Cu1 and (c) PPy@Ag/Cu5 hybrid nanocomposite.
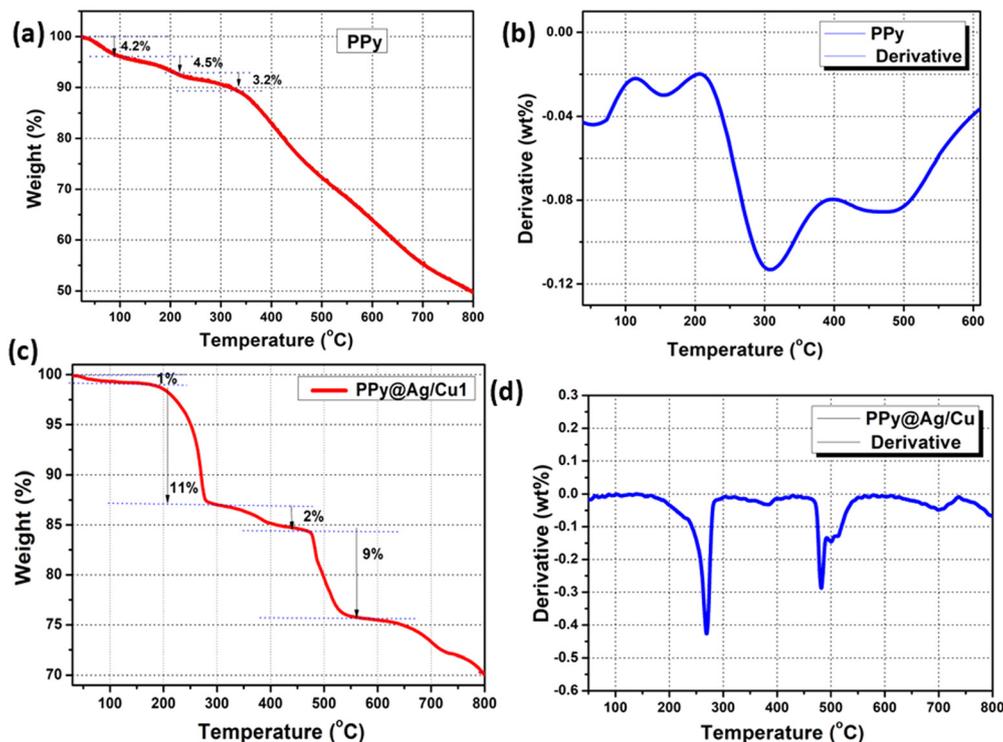
Fig. 10 TG-DTA of (a) and (b) PPy and (c) and (d) the PPy@Ag/Cu hybrid nanocomposite.

representing further polymer degradation and interaction between PPy and the Ag/Cu nanoparticles. Beyond 550 °C, the weight stabilizes, indicating the complete decomposition of the organic components, leaving behind the Ag and Cu nanoparticles. A small residual weight remains, corresponding to the metal oxide content, which confirms the presence of silver and copper. Fig. 10d indicates that DTA measures the exothermic/endothermic temperature difference between the PPy@Ag/Cu nanocomposite. According to the initial weight loss shown in the TGA curve (Fig. 10c), the evaporation of absorbed moisture corresponds to the endothermic peak at 278 °C. As the PPy@Ag/Cu nanocomposite degrades under heat, an exothermic peak appears at 743 °C. This breakdown of metal-doped polymer chains releases energy, making it an exothermic reaction. Higher endothermic peaks at 482 °C suggest further stages of disintegration of the PPy@Ag/Cu hybrid nanocomposite interactions. This observation could potentially point to the oxidation of the residues of Ag/Cu nanoparticles. Here, we show that the PPy@Ag/Cu1 hybrid nanocomposite is remarkably stable within the temperature range of the thermal conductivity experiments using TGA and DTA data.

3.7 Gas sensing studies

The gas response was measured using a specifically designed gas chamber and a static mode was used for the gas sensing readings. After development, the sensor was placed in the gas chamber, and by using a syringe, a specified amount of test gas was delivered into the chamber until the gas concentration (in parts per million) was achieved. Recovery of the sensor was

recorded by exposing it to fresh air once steady state had been achieved. In addition to activating the vacuum pump, the chamber's input and exit valves were simultaneously opened. Gas may be introduced into the chamber through the inlet valve and released through the outlet valve. The degassing process was expedited by the vacuum pump and everything was done at room temperature for measuring gas sensitivity, as shown in Fig. 11. The required concentration of the gas is prepared by the static gas distribution method given by the formula[18]

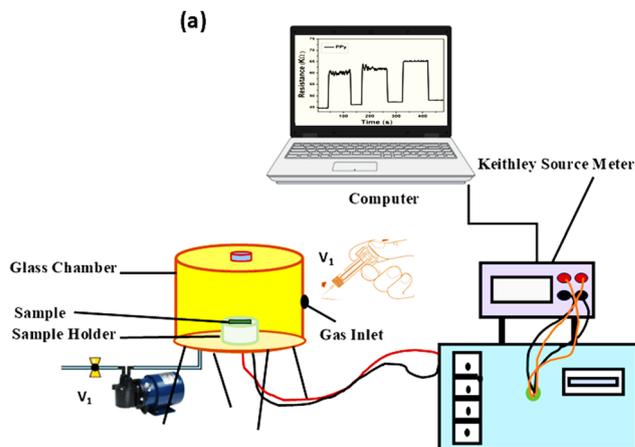$$C(\text{ppm}) = \frac{22.4 \, \rho TV'}{273 \, MV} \times 1000 \qquad (5)$$

Fig. 11 Schematic diagram of a gas sensing experimental setup.

where C(ppm) is the desired target gas concentration, ρ is (g mL^{-1}) the density of the liquid (gas), V' is the volume of gas, T is temperature in Kelvin, M is molecular weight of the gas (g mol^{-1}), and V is the volume of the chamber (L). The humidity present inside the chamber and temperature reading on the day of experiment were 50% and $\sim$27 °C, respectively. The performance of the sensor response was evaluated using:

$$R\% = \frac{R_a - R_g}{R_g} \times 100 \qquad (6)$$

where R_a is the electrical resistance in clear air and R_g is the resistance in the test gas. Assessing sensor response and recovery times are the next key elements to evaluate. The reaction time is the amount of time that passes between gas consumption and a discernible change in the parameter, whereas the recovery time is the amount of time it takes for the parameter to return to its initial value following gas removal. They can be measured in two ways: first, the time it takes the sensor to obtain 90% saturation of R_g from R_a during gas intake, and second, the value of R_a at 10% during gas withdrawal. The sensor is able to respond to NH$_3$ gas by modulating the response/recovery time between different concentrations of metal doped and various amounts of NH$_3$ gas. According to the IUPAC, sensitivity is defined as the slope of the calibration curve (sensing response *versus* target gas concentration):

$$S = \Delta R/\Delta C \qquad (7)$$

here ΔR and ΔC are the change in sensor response and concentration.

3.7.1 Gas sensing response and sensitivity. The sensor's ability to respond to NH$_3$ gas is facilitated by the modulation of the response/recovery cycle in response to various concentrations of metal-doped atoms. The detection range of 100–300 ppm for NH$_3$ gas is illustrated in Fig. 12 in proportion to the sensor resistance. The resistance values of sensors formed from PPy and PPy@Ag/Cu hybrid nanocomposite film with varying concentrations of doped metal are observed to decrease abruptly as the concentration of NH$_3$ gas increases (Fig. 12a). The resistance of the synthetic sensors for 100 ppm of ammonia gas varies from 21.4 KΩ to 56.4 KΩ for the PPy@Cu/Ag1 hybrid nanocomposite; 19.6 KΩ to 52.3 KΩ for the PPy@Ag/Cu2 hybrid nanocomposite; 18.3 KΩ to 52.2 KΩ for the PPy@Ag/Cu3 hybrid nanocomposite; 18.5 KΩ to 56.1 KΩ for the PPy@Ag/Cu4 hybrid nanocomposite and 16.4 KΩ to 53.2 KΩ for the PPy@Ag/Cu5 hybrid nanocomposite, and from 44.2 KΩ to 65.3 KΩ for the pure PPy sensor. Fig. 12b shows the sensing responses against concentration to find the sensitivity of the sensor. For the PPy@Ag/Cu1–PPy@Ag/Cu5 hybrid nanocomposite film, the numerical value falls within the range of 0.025–0.02 ppm^{-1}, and the slope has been calculated by fitting the curve linearly. The PPy@Ag/Cu hybrid nanocomposite demonstrates enhanced sensitivity compared to PPy due to

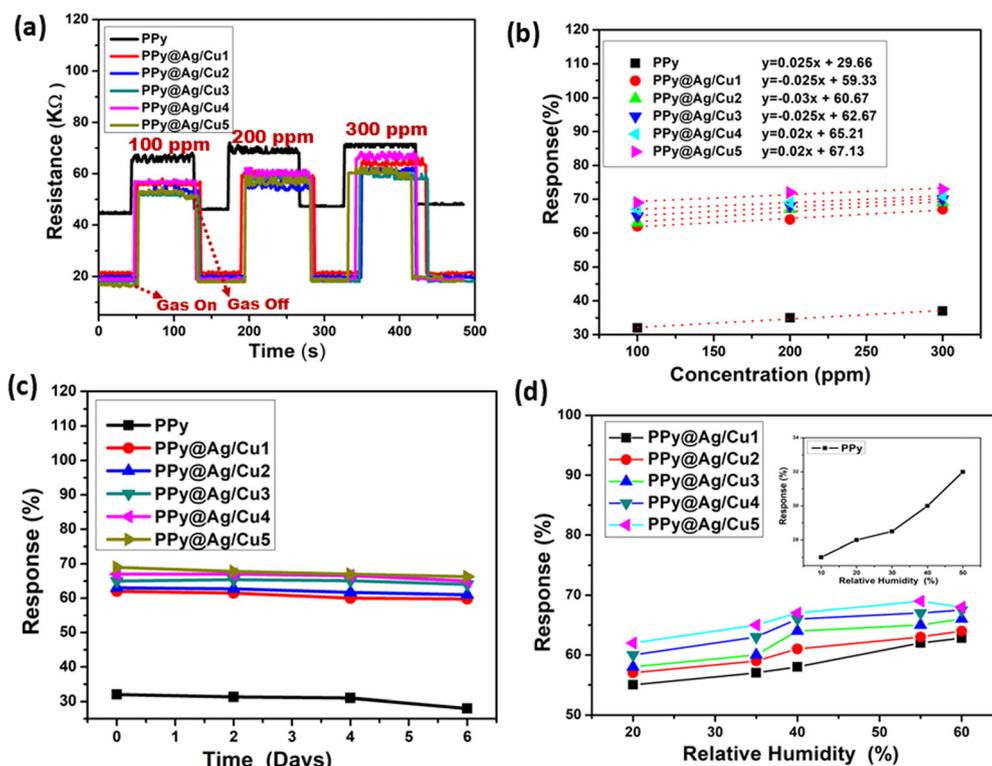**Fig. 12** (a) Resistance of gas sensors based on PPy and the PPy@Ag/Cu1–5 hybrid nanocomposite film when exposed to various concentrations of NH$_3$ gas at room temperature, (b) sensitivity of PPy and its hybrid nanocomposite film, (c) stability of the gas sensor based on PPy and its nanocomposite film toward 100 ppm ammonia and (d) effect of humidity on the prepared sensor when exposed to 100 ppm ammonia.

the synergistic effects of Ag and Cu nanoparticles within the PPy matrix. First, the incorporation of Ag and Cu nanoparticles significantly increases the surface area and the number of active sites available for gas adsorption, leading to a more efficient interaction between the gas molecules and the sensor surface. The presence of Ag and Cu enhances the charge transfer between the nanocomposite and the target gas molecules, facilitating a faster and more pronounced change in the electrical conductivity of PPy. Additionally, both Ag and Cu have catalytic properties, which can lower the activation energy for the adsorption and reaction of gas molecules, further improving sensitivity. The combination of these two metals in the nanocomposite allows for the formation of heterojunctions, which contribute to improved electron mobility and enhanced sensing performance. Furthermore, Ag and Cu nanoparticles can influence the morphology and porosity of the PPy matrix, creating a more porous structure that allows for better diffusion of gas molecules into the composite. The enhanced catalytic behaviour, increased surface area, and improved charge transfer in the hybrid nanocomposite collectively lead to greater sensitivity compared to pure PPy.

Table 4 provides the response values, so we can see how the sensors used in this study react to varying concentrations of ammonia gas. We also observed the sensor response of the PPy and PPy@Ag/Cu1–5 hybrid nanocomposite gas sensors during up to seven days of exposure to NH_3 gas, as illustrated in Fig. 12c, which shows that the sensors maintain consistent performance over this period. The PPy and PPy@Ag/Cu nanocomposite active sites and the ammonia molecules' robust interaction are likely responsible for the sensor response's stability over time. This interaction enables the material to undergo repeated adsorption and desorption cycles without significant degradation. After seven days, there may be a slight decrease in response as a result of factors such as minor surface saturation, and subtle changes in the active surface area such as the oxidation state of the copper. Nevertheless, this reduction is negligible, suggesting that the sensor's structural

and functional integrity are largely unaffected. Consequently, the sensors that have been prepared are suitable for continuous ammonia detection applications. In addition, we have investigated the impact of humidity on the efficacy of the PPy and PPy@Cu1–5 hybrid nanocomposite film when it is exposed to 100 ppm of NH_3 gas in various humid conditions.

Fig. 12d shows the sensor's response to different humidity levels. If the relative humidity rises, the sensor will give a stronger indication. The sensor responds most accurately when the relative humidity (RH%) is 50% for PPy and 55% for the PPy@Ag/Cu hybrid nanocomposite. At 55% RH, the PPy@Ag/Cu hybrid nanocomposite film shows its most accurate response because this level of humidity likely provides an optimal balance between the availability of water molecules and the adsorption of NH_3. The presence of water can facilitate charge transfer processes and improve the sensor's conductivity, leading to a stronger and more accurate indication of NH_3 gas. Beyond this point, at 60% RH, the sensor still performs well but may start to exhibit a slightly different response due to excess water molecules possibly beginning to block active sites or alter the surface properties, which could affect gas diffusion and interaction. This phenomenon suggests that the sensor material benefits from moderate humidity levels, where water enhances the sensing mechanism without overwhelming the active sites, leading to an overall improvement in performance at higher but controlled humidity levels.

3.7.2 Response and recovery time. In Fig. 13, the response (T_1 (s)) and recovery time (T_2 (s)) of the PPy and PPy@Ag/Cu hybrid nanocomposite are illustrated for a variety of NH_3 gas volumes. As the concentration of NH_3 grew from 100 ppm to 300 ppm, the response time increased from 37 s to 39 s for PPy and in contrast, the response time of the PPy@Ag/Cu1 nanocomposite decreases to 17 s, while the recuperation time improves to 18 s. Due to the presence of Ag and copper ions in the PPy matrix, the PPy@Ag/Cu hybrid nanocomposite film exhibits a rapid recovery period. Although the PPy@Ag/Cu3 nanocomposite film has a minimum response time of

Table 4 Comparison of the PPy@Ag/Cu hybrid nanocomposite film-based gas sensor and those reported in the literature

| Material	Multicomponent		Substrate	Temp.	Gas	ppm	Response (%)	T_1 (s)	T_2 (s)	Ref.
PPy	Ag	SnO_2	IDEs	RT	NH_3	0.02	3.15	–	–	19
PPy	TiO_2	Graphene	ITO	RT	NH_3	50	102.2	36	16	20
PPy	Pd	CNT	IDEs	RT	H_2	10	~4.5	<1	<1	21
PPy	Au	TiO_2	IDEs	RT	NH_3	0.02	3.2			19
PPy@Ag/Cu1	Ag	Cu	Si	RT	NH_3	100	62	17	18	This work
						200	64	15	17	
						300	67	13	14	
PPy@Ag/Cu2	Ag	Cu	Si	RT	NH_3	100	63	16	14	This work
						200	67	15	12	
						300	69	13	11	
PPy@Ag/Cu3	Ag	Cu	Si	RT	NH_3	100	65	15	13	This work
						200	68	14	11	
						300	70	11	12	
PPy@Ag/Cu4	Ag	Cu	Si	RT	NH_3	100	67	16	14	This work
						200	69	15	12	
						300	71	14	13	
PPy@Ag/Cu5	Ag	Cu	Si	RT	NH_3	100	69	13	12	This work
						200	72	12	10	
						300	73	11	11	
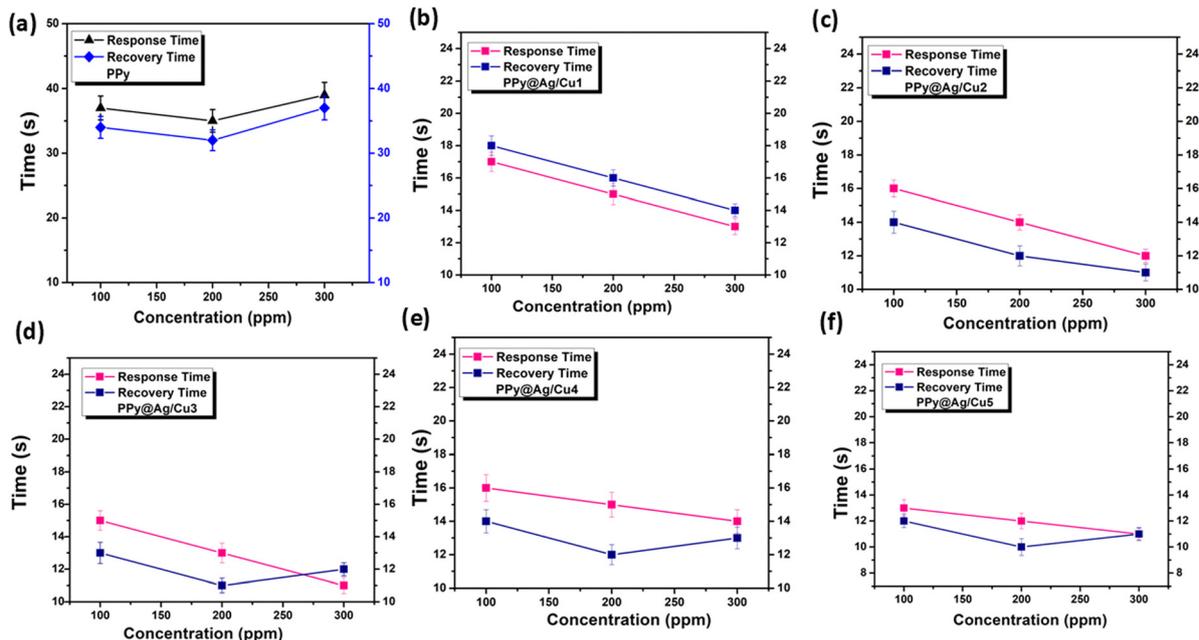
Fig. 13 Response–recovery curves of gas sensors based on the (a) PPy and (b) and (f) PPy@Ag/Cu hybrid nanocomposite film when exposed to various concentrations of NH_3 gas at room temperature.

approximately 11 s at 300 ppm. The significant sensitivity to NH_3 gas exhibited by the PPy@Ag/Cu sensor with a high doping concentration may be attributed to its accelerated oxidation rate. Fig. 12 illustrates that the sensitivity, film response, and recovery time of the nanocomposites can be enhanced by adjusting the concentrations of silver and copper in the PPy matrix. The chemical polymerisation of PPy agglomeration of nano spheroids onto silver and copper may be the cause of the excellent response and recovery times. This procedure results in an increased surface area and a more uniform distribution of the agglomeration of nano spheroids, which in turn enhances the ammonia gas sensing efficacy at room temperature. In 3.4 we investigated the integration of morphology and nanostructure investigations into PPy@Ag/Cu hybrid nanocomposites to determine the most effective way of increasing the number of active sites for the adsorption of NH_3 gas molecules. This, in

turn, reduced the recovery time and response time. Table 4 provides a concise summary of the research conducted on NH_3 gas sensors and the comparison between the PPy@Ag/Cu hybrid nanocomposite film and other sensors.

3.7.3 Selectivity of the PPy@Ag/Cu hybrid nanocomposite film. The PPy and PPy@Ag/Cu hybrid nanocomposite films were exposed to selectivity testing in this study. As shown in Fig. 14, the PPy and PPy@Ag/Cu1 hybrid nanocomposite sensor responded to 100 ppm concentrations of NH_3 gas, ethanol (C_2H_5OH), carbon monoxide (CO), hydrogen sulphide (H_2S), and carbon dioxide (CO_2), respectively. When compared to the other gases analysed, the PPy and its hybrid nanocomposite sensor clearly react much more strongly to NH_3 gas. Ammonia is a highly reactive, polar gas with lone pairs of electrons on its nitrogen atom. These lone pairs can interact effectively with the PPy matrix, particularly through charge transfer processes. The
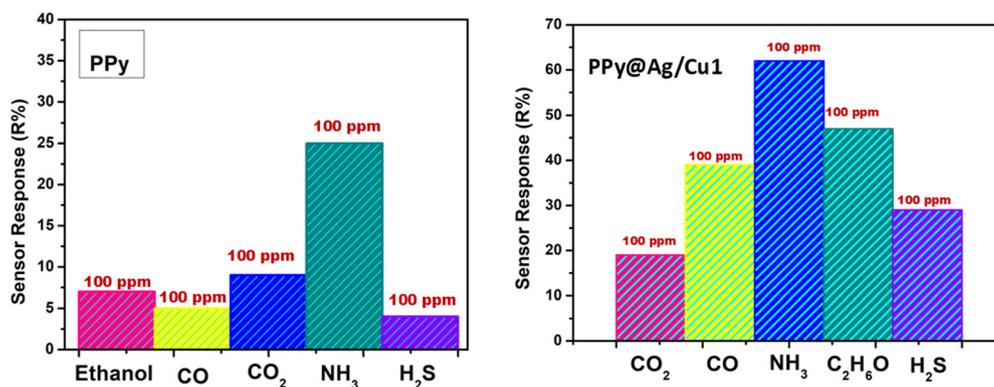

Fig. 14 Selectivity of PPy and its hybrid nanocomposite gas sensor.

presence of Ag and Cu nanoparticles in the composite enhances this effect by increasing the number of active sites and promoting catalytic behavior. Silver, in particular, has known catalytic activity that can further amplify the sensor's response to NH_3. Moreover, NH_3 is a basic gas, which tends to interact strongly with the acidic nature of PPy, leading to a significant change in the electrical properties of the sensor. This interaction causes a noticeable shift in conductivity, which is detected as a stronger sensor response. In contrast, the other gases analysed (C_2H_5OH, CO, H_2S, CO_2) either lack the same level of interaction with the sensor material or do not induce significant changes in the conductivity due to weaker adsorption or non-polar behaviour. Thus, the high sensitivity of the PPy@Ag/Cu1 sensor to NH_3 results from a combination of strong adsorption, effective charge transfer, and enhanced catalytic activity, making it much more responsive to ammonia than to the other gases tested.

3.7.4   Sensing mechanism of the PPy@Ag/Cu hybrid nanocomposite. The sensing mechanism of the PPy@Ag/Cu hybrid nanocomposite towards NH_3 gas is primarily based on changes in electrical conductivity resulting from the interaction between the gas molecules and the sensor material. PPy is a conducting polymer, and when NH_3 gas comes into contact with it, a charge transfer process occurs due to ammonia's basic nature and the lone pairs of electrons on its nitrogen atom (Fig. 15a). NH_3 molecules tend to donate electrons to the PPy matrix, which leads to a reduction in the concentration of charge carriers in the polymer. This electron donation decreases the overall conductivity of the PPy. The presence of Ag and Cu nanoparticles in the nanocomposite further enhances this sensing mechanism. Ag and Cu nanoparticles increase the number of active sites for gas adsorption and may exhibit catalytic behaviour, which amplifies the interaction between NH_3 and the PPy matrix.[22,23] This results in a more pronounced conductivity change upon exposure to ammonia. The hybrid structure, combining conducting PPy with metallic Ag and Cu, facilitates better charge transfer and gas adsorption. Additionally, the

metallic nanoparticles help in improving the sensitivity and selectivity of the sensor towards ammonia, as the interaction with NH_3 gas disrupts the electrical balance within the nanocomposite. The outcome is a measurable change in electrical resistance, which is detected as the sensor's response to ammonia. Thus, the PPy@Ag/Cu hybrid nanocomposite effectively translates the chemical interaction with NH_3 into an electrical signal, allowing for sensitive ammonia gas detection.

The energy band diagram of the PPy@Ag/Cu hybrid nanocomposite during ammonia (NH_3) gas sensing illustrates the changes in the electronic structure of the material upon interaction with ammonia molecules. PPy has a typical band structure with a valence band (occupied by electrons) and a conduction band (where charge carriers move) (Fig. 15b). Between these bands is the bandgap, which dictates the material's conductivity. When the PPy@Ag/Cu nanocomposite is exposed to ammonia gas, electron donation from NH_3 molecules plays a crucial role in altering the energy bands. The nitrogen atoms in NH_3, possessing lone pairs of electrons, donate these electrons to the PPy matrix. This electron donation leads to an increase in electron density in the conduction band, effectively reducing the number of charge carriers on the PPy, thus lowering its conductivity. The inclusion of Ag and Cu nanoparticles in the nanocomposite modifies the energy band structure by creating additional energy states or trap sites within the bandgap. These metal nanoparticles provide active sites for gas adsorption and act as electron sinks or donors depending on the interaction with the gas molecules. During ammonia gas sensing, the Ag and Cu nanoparticles facilitate electron transfer between NH_3 and the PPy matrix, leading to a significant shift in the Fermi level.[24] The Fermi level moves closer to the conduction band due to the electron donation from NH_3, which further affects the charge transport properties of the nanocomposite. This band alignment between PPy and the Ag/Cu nanoparticles enhances the gas sensing performance by allowing efficient electron exchange, thereby improving the sensitivity and selectivity of the sensor. As ammonia adsorbs
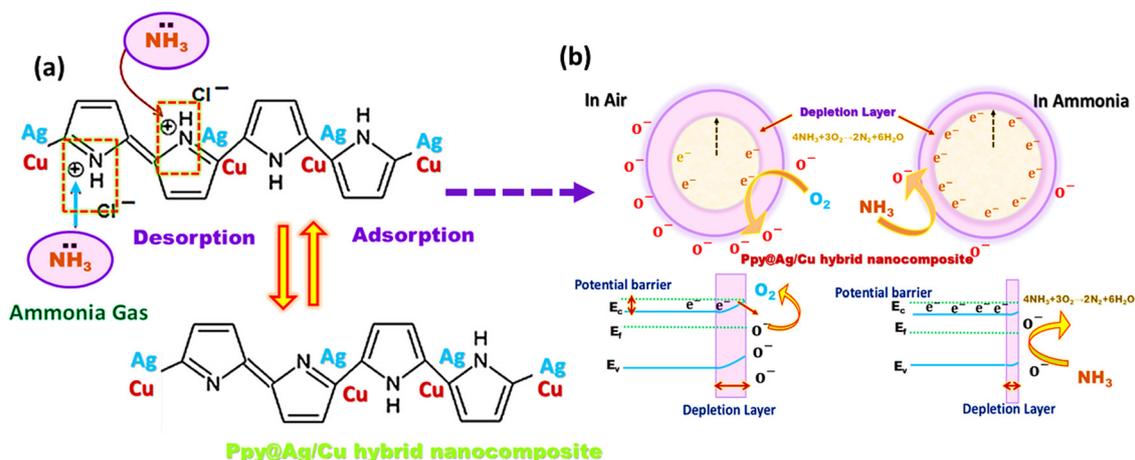

Fig. 15   (a) Schematic of the ammonia sensing mechanism of sensors based on the PPy@Ag/Cu hybrid nanocomposite; (b) energy band diagram of the PPy@Ag/Cu hybrid nanocomposite during the gas sensing reaction process.

onto the surface, the energy barrier for electron transport increases, causing a detectable change in the sensor's electrical properties. This shift in the energy bands due to NH_3 adsorption is responsible for the measurable variation in conductivity that characterizes the sensor's response.

4. Conclusion

In conclusion, PPy@Ag/Cu hybrid nanocomposites were synthesized through chemical oxidative polymerization of the pyrrole monomer for application as gas sensors. The concentrations of Ag and Cu nanoparticles were varied to identify the optimal composition for ammonia detection. Among the synthesized samples, the PPy@Ag/Cu5 nanocomposite thin film demonstrated the highest response of $\sim 73\%$ for 300 ppm ammonia, with response and recovery times of 11 seconds each. This suggests that increasing the Ag and Cu concentrations enhances the ammonia gas sensing performance at room temperature. The improved sensing performance of the PPy@Ag/Cu hybrid nanocomposite can be attributed to the synergistic effects of conductivity changes, protonation, and interactions with the embedded metal nanoparticles. These factors contribute to the high sensitivity and selectivity of the nanocomposite in detecting ammonia gas. However, this study tested the sensors over a limited range of gas concentrations, and real-world applications may require broader and more variable ranges. Additionally, the selectivity of the sensor towards ammonia in the presence of other interfering gases has been extensively investigated. Finally, the long-term stability and durability of the PPy@Ag/Cu nanocomposite sensors show good results for practical applications.

Data availability

The data used to support the findings of this study are available from the corresponding author upon request.

Conflicts of interest

The authors declare no conflicts of interest.

References

1 A. Verma and T. Kumar, PANI@Ag nanocomposites gas sensors for rapid detection of ammonia, *Polyhedron*, 2024, 116982.

2 A. S. Roy, A. R. Koppalkar and M. V. N. A. Prasad, *J. Appl. Polym. Sci.*, 2011, **121**(2), 675.

3 A. S. Roy, S. G. Hegde and A. Parveen, *Polym. Adv. Technol.*, 2014, **25**(1), 130.

4 A. Parveen, A. R. Koppalkar and A. S. Roy, *IEEE Sens. J.*, 2012, **12**(9), 2817.

5 A. Parveen, A. R. Koppalkar and A. S. Roy, *Sens. Lett.*, 2013, **11**(2), 242.

6 A. Verma, *et al.*, Review—Recent Advances and Challenges of Conducting Polymer-Metal Nanocomposites for the Detection of Industrial Waste Gases, *ECS J. Solid State Sci. Technol.*, 2023, **12**, 047002.

7 A. Verma and T. Kumar, Ag/Cu doped polyaniline hybrid nanocomposite-based novel gas sensor for enhanced ammonia gas sensing performance at room temperature, *RSC Adv.*, 2024, **14**, 25093–25107.

8 A. Verma and T. Kumar, Gas sensing properties of a Cu-doped PANI nanocomposite towards ammonia, *Mater. Adv.*, 2024, **5**, 7387–7400.

9 S. Anuradha, A. S. Roy and M. V. N. A. Prasad, Synthesis, characterization, and microwave properties of polypyrrole/molybdenum trioxide composites, *Sci. Eng. Compos. Mater.*, 2014, **21**(4), 479–483.

10 M. Gerard, A. Chaubey and B. D. Malhotra, *Biosens. Bioelectron.*, 2002, **17**(5), 345–359.

11 H. J. Akber, *et al.*, Sensing Characteristics of Nanostructured PANI/Ag Thin Films as H_2S Gas Sensor, *Mater. Sci. Eng.*, 2020, **928**, 072146.

12 P. Mokhtari, J. Hadi and A. Majedi, *J. Polym. Res.*, 2014, **21**, 491.

13 Y. Wang, S. Li and G. Wu, *Sens. Actuators, B*, 2010, **144**(1), 220–225.

14 N. Chaudhari and S. Patil, *J. Appl. Polym. Sci.*, 2018, **135**(17), 46210.

15 J. Chen, C. O. Too, G. G. Wallace and G. F. Swiegers, *Electrochim. Acta*, 2004, **49**, 691.

16 H. Wei, W. Zhang and Y. Ma, *J. Mater. Sci.*, 2016, **51**, 1065–1075.

17 S. Dhibar and C. K. Das, Transition metal-doped polyaniline/single-walled carbon nanotubes nanocomposites: Efficient electrode material for high performance supercapacitors, *Ind. Eng. Chem. Res.*, 2014, **53**, 3495–3508.

18 P. Dipak, D. C. Tiwari and A. Samadhiya, *et al.*, Synthesis of polyaniline (printable nanoink) gas sensor for the detection of ammonia gas, *J. Mater. Sci.: Mater. Electron.*, 2020, **31**, 22512–22521, DOI: 10.1007/s10854-020-04760-2.

19 T. Jiang, Z. Wang and Z. Li, *et al.*, Synergic effect within n-type inorganic–p-type organic nano-hybrids in gas sensors, *J. Mater. Chem. C*, 2013, **1**, 3017.

20 C. Xiang, D. Jiang and Y. Zou, *et al.*, Ammonia sensor based on polypyrrole–graphene nanocomposite decorated with titania nanoparticles, *Ceram. Int.*, 2015, **41**, 6432–6438.

21 S. J. Park, O. S. Kwon and J. Jang, A high-performance hydrogen gas sensor using ultrathin polypyrrole-coated CNT nanohybrids, *Chem. Commun.*, 2013, **49**, 4673–4675.

22 D. Shan, J. Wang and X. Xue, *J. Nanomater.*, 2013, 451950.

23 N. Roy and A. A. Ansari, *Sens. Actuators, B*, 2011, **160**(1), 433–442.

24 Y. Wang, *J. Phys. Chem. C*, 2009, **113**(27), 11696–11702.